

[Click here to download Manuscript: Browne et al revised manuscript.docx](#)

A computational model of inhibition of HIV-1 by interferon-alpha

Edward P Browne^{1*}, Benjamin Letham² and Cynthia Rudin^{2,3,4}.

¹Koch Institute for Integrative Cancer Research, ²Operations Research Center,

³Sloan School of Management, ⁴Computer Science and Artificial Intelligence

Laboratory, Massachusetts Institute of Technology

***ebrowne@mit.edu**

Abstract:

Type 1 interferons such as interferon-alpha (IFN α) inhibit replication of Human immunodeficiency virus (HIV-1) by upregulating the expression of genes that interfere with specific steps in the viral life cycle. This pathway thus represents a potential target for immune-based therapies that can alter the dynamics of host-virus interactions to benefit the host. To obtain a deeper mechanistic understanding of how IFN α impacts spreading HIV-1 infection, we modeled the interaction of HIV-1 with CD4 T cells and IFN α as a dynamical system. This model was then tested using experimental data from a cell culture model of spreading HIV-1 infection. We found that a model in which IFN α induces reversible cellular states that block both early and late stages of HIV-1 infection, combined with a saturating rate of conversion to these states, was able to successfully fit the experimental dataset. Sensitivity analysis showed that the potency of inhibition by IFN α was particularly dependent on specific network parameters and rate constants. This model will be useful for designing new therapies targeting the IFN α network in HIV-1-infected individuals, as well as potentially serving as a template for understanding the interaction of IFN α with other viruses.

Author Summary

Interferon-alpha (IFN α) is a key component of the host response to HIV-1, but the details of how IFN α regulates infection are still incompletely understood. To provide a deeper understanding of the dynamics of how IFN α inhibits HIV-1, we simulated the interaction of IFN α and HIV-1 as a computational model and compared this model to an experimental dataset. We identify a model structure that is able to fit many key features of the data. Furthermore, we use the model to predict optimal strategies for targeting the IFN α pathway therapeutically. We anticipate that this model will be useful for further analysis of HIV-IFN α interactions and will help to guide new therapeutic strategies.

Introduction:

Around 65 million people worldwide have been infected with Human immunodeficiency virus (HIV-1) [1]. Although progress has been made in mitigating disease with antiviral chemotherapy, a protective vaccine has proved elusive, and other approaches are still needed. Furthermore, permanently eliminating virus from patients undergoing drug therapy has been difficult due to the existence of latently infected reservoirs that are resistant to standard antiviral therapy [2]. Another possible approach to treating HIV-1 infection is to alter aspects of virus-host dynamics by targeting host pathways that inhibit or enhance infection. For this to be successful, a deep understanding of the dynamics underlying how specific host pathways interact with HIV-1 will likely be required.

The application of mathematical modeling to HIV-1 dynamics during acute and chronic infection has been highly successful at improving our understanding of the basic features of clinical infection. In particular, fundamental insights into the response to antiviral therapy, and the existence of multiple long-lived virus reservoirs have been revealed [3–6]. In early models, the extent of infection was typically limited by target cell abundance, although more recent HIV-1 models have also considered the impact of virus-specific CD8 T cells [7,8]. However these models have not yet included the impact of the host innate immune system.

A key component of the host innate response to HIV-1 infection is the type 1 interferon (IFN) system [9,10]. In humans, type 1 IFNs consist of a family of related cytokines including 13 subtypes of IFN α , and two subtypes of IFN β , that are secreted in response to stimulation of microbe-sensing pattern-recognition receptors such as Toll-like receptors (TLRs), RIG-I-like receptors (RLRs) and NOD-like receptors (NLRs) [11]. Type 1 IFNs bind the IFN α receptor (IFNAR) and activate phosphorylation of the signaling molecules STAT1 and STAT2, which then bind to Interferon regulatory factor 9 (IRF9) to form the Interferon-stimulated gene factor 3 (ISGF3) complex [12]. ISGF3 then binds to conserved Interferon-sensitive response elements (ISREs) found upstream of interferon-sensitive genes (ISGs) [13]. Dozens of ISGs are upregulated by IFN α , the function of which only a few are clearly understood [14]. Overall, IFNs create an antiviral state that can either prevent *de novo* infections, or inhibit later stages of virus replication in cells, such as assembly and egress.

IFN α is detectable in the plasma during acute HIV-1 infection, and this cytokine is predominantly secreted by plasmacytoid dendritic cells (pDCs). pDCs detect HIV-1 via the single-stranded RNA sensor TLR7, and secrete high levels of IFN α due to constitutive expression of the Interferon regulatory factor 7 (IRF7) transcription factor [15,16]. A number of ISGs have been shown to have anti-HIV-1 activity [17]. In particular, Tripartite motif-containing 22 (TRIM22) and Myxovirus resistance protein 2 (MX2) inhibit early stages of infection [18,19], while other ISGs such as Apolipoprotein B mRNA editing enzyme, catalytic polypeptide-like 3G (APOBEC3G) and Tetherin target later stages of infection, such as virus release or the infectivity of virus particles [20,21]. Furthermore, IFN α inhibits HIV-1 replication in tissue culture and blockade of IFN α during Simian immunodeficiency virus (SIV) infection leads to higher virus levels *in vivo* [10].

Due to its HIV-1-inhibiting properties, IFN α has attracted interest as a therapeutic target for HIV-1 infection. However, treatment of HIV-1 patients with recombinant IFN α has produced inconsistent and disappointing results, with only modest effects on virus levels being observed [22–24]. However, since the structure of the IFN α inhibitory network, as well as the parameters that regulate its activity are poorly understood, a better understanding of the underlying dynamics of this response may lead to improved and more effective IFN α -based therapies. For example, dynamical models may help pinpoint which molecular components of the IFN α inhibition network will achieve the most potent or most durable results. Furthermore, modeling approaches have previously

been applied to the interaction of Hepatitis C virus (HCV) with peggylated IFN α , and have yielded valuable insights [25–27].

To achieve this goal, we simulated the inhibition of HIV-1 by IFN α using a dynamical system modeling approach, and tested this model in a well-defined experimental system. In our model, IFN α interacts with both HIV-1-infected and uninfected cells to induce a reversible state of blocked infection, and we demonstrate that this model makes testable predictions about how specific network parameters may be targeted to achieve maximal inhibition of HIV-1.

Results:

IFN α inhibits spreading HIV-1 infection.

To generate an experimental dataset against which different models can be tested, we performed experiments with a tissue culture model of spreading HIV-1 infection. CEM-5.25 cells are a human CD4 T cell line that are susceptible to HIV-1 infection and contain an integrated HIV-1 long terminal repeat-Green fluorescent protein (LTR-GFP) reporter cassette [28]. Infected cells express GFP due to the viral Tat protein permitting transcription of GFP from the integrated LTR. This allows us to distinguish HIV-1-infected cells (GFP+) from uninfected cells (GFP-). CEM-5.25 cells were infected with HIV-1, and both cell and supernatant samples were then isolated at 24h intervals for 72h post infection. Cells samples were analyzed by flow cytometry to determine 1) absolute

cell numbers and 2) the percentage of HIV-1-infected (% GFP+) cells. Infectious virus in the supernatant was quantified by focus-forming assay using GHOST-X4 reporter cells [29]. In infected cell cultures, the % GFP+ cells, as well as the concentration of infectious HIV-1 in the supernatant, rises exponentially until 3dpi (Fig. 1B,C). By day 3, total cell levels decline due to infection-induced cytopathic effect (Fig. 1A).

Figure 1: Inhibition of spreading HIV-1 infection by IFN α .

A human CD4 T cell line was infected with HIV-1 and the total concentration of cells (A), the proportion of infected (GFP+) cells (B), and the concentration of infectious virus in the supernatant (C), were monitored at 24h intervals. Different concentrations of IFN α were added to the cells at 6h prior to infection, and the effect on total cell concentration (D), the percent infected cells (E), and the concentration of infectious HIV-1 in the supernatant (F), were measured every 24h. Measurements were taken in quadruplicate and data shown are representative of three independent experiments. Error bars represent the standard deviation of the dataset.

To examine the effect of IFN α on the replication of HIV-1 in this system, different concentrations of IFN α were included in the tissue culture media from 6h prior to infection and maintained throughout the course of the infection. Inclusion of IFN α in the media caused a clear and progressive decrease in the accumulation of infected cells (Fig. 1E) and infectious HIV-1 in the supernatant (Fig. 1F), as well and an increase in overall cell density at later timepoints (Fig 1D). Interestingly, inhibition of HIV-1 by IFN α exhibits two key features – firstly that the inhibition curve is very broad – with

differential inhibition being observed for IFN α concentrations over several orders of magnitude (from 2pg/mL to 20ng/mL), and secondly, that inhibition of HIV-1 increased only minimally above 2ng/mL, suggesting that inhibition saturates at higher IFN α concentrations. 50% inhibition of infection, as measured by infectious HIV-1 concentration at 3dpi, was achieved between at 0.02ng/mL and 0.2ng/mL (Fig. 1F).

Model of IFN α inhibitory network.

We constructed a dynamical system that models the dynamics of CD4 T cells and their interaction with both HIV-1 and IFN α (Fig. 2, Table 1). This model shares a number of features with a model previously used to analyze the IFN α response to influenza infection [30]. In this system, the initial species are HIV-1 (H), CD4 T cells (C) and IFN α (I). HIV-1 can infect CD4 T cells to generate infected cells (CH) at a rate proportional to the concentrations of HIV-1 and CD4 T cells, *via* the infection rate constant (k_5). Infected cells secrete infectious HIV-1 (H) at a constant rate (k_6). IFN α can bind to uninfected (C) or infected cells (CH) and convert them into refractory cells (CI) that cannot be infected, or infected-inhibited cells (CHI) that no longer release virus, respectively. The rate of this conversion is determined by the concentrations of susceptible cells and IFN α , as well as the k_2 and k_8 rate constants. Since the effects of IFN α on cells are reversible, CI and CHI revert at an intrinsic rate (k_3) to C or CH respectively. H and I each have their own intrinsic decay rates that were measured separately (k_7 and k_9) (Fig. S1). For these studies, an immortalized CD4 T cell line (CEM 5.25) was used that divides continuously and has an intrinsic death rate that is negligible when maintained at subconfluency. By contrast, HIV-1-infected cells (CH and CHI) cells die at an intrinsic rate due to the

cytopathic effect of HIV-1 infection (k_4). All CD4 T cell subsets divide at an intrinsic rate to generate additional cells of the same type. The replenishment rate of all CD4 T cells was modeled with the same rate for all subspecies (k_1), which was experimentally determined by parameter fitting.

Figure 2: Model of inhibition of HIV-1 by IFN α .

CD4 T cells are replenished at a rate proportional to the number of cells, leading to exponential growth (k_1). HIV-1 particles infect cells (k_5), and infected cells die at an inherent rate (k_4). IFN α inhibits infection by converting uninfected cells (C) and infected cells (CH) into states in which they cannot be infected (CI), or which longer release infectious virus (CHI) (k_2), and this rate is also governed by a saturating rate constant (k_8). Both these states are reversible, and without continued IFN α exposure, CI and CHI revert to C and CH respectively (k_3). Infected cells (CH) secrete HIV-1 at a continuous rate (k_6). Both HIV-1 and IFN α have their own natural decay rates (k_7 and k_9 respectively).

Table 1: Species and parameter descriptions.

Species/parameter	description	Units
C	Uninfected CD4 T cells	cells μL^{-1}
CI	Uninfected CD4 T cells made refractory to infection by IFN α	cells μL^{-1}
CH	HIV-1-infected CD4 T cells	cells μL^{-1}
CHI	HIV-1-infected CD4 T cells in which virus release	cells μL^{-1}

	has been blocked by IFN α	
H	HIV-1	Focus-forming units (FFU) uL ⁻¹
I	Interferon alpha	ng mL ⁻¹
k ₁	Intrinsic division rate of CD4 T cells	day ⁻¹
k ₂	Rate of conversion of CD4 T cells to refractory (CI) or blocked (CHI) state.	ng ⁻¹ day ⁻¹
k ₃	Intrinsic rate of reversion of IFN α exposed cells to HIV-1 susceptible state.	day ⁻¹
k ₄	Death rate for HIV-1 infected cells (CH and CHI)	day ⁻¹
k ₅	Infection rate	uL day ⁻¹ FFU ⁻¹
k ₆	HIV-1 secretion rate from infected cells (CH)	FFU cell ⁻¹ day ⁻¹
k ₇	HIV-1 decay rate	day ⁻¹
k ₈	Saturated rate of conversion to CI or CHI	ng mL ⁻¹
k ₉	IFN α activity decay rate	day ⁻¹

One key element of our model was the inclusion of a Michaelis-Menten saturating rate constant (k_8) for the conversion of C to CI and CH to CHI. As such, the conversion rate of C to CI and CH to CHI saturates for high I concentrations, due to k_8 . Previous models of IFN α interaction with virus infection do not include saturation for conversion to an inhibited state [30], and this therefore represents a novel feature of this model.

Our system of equations is thus:

$$\begin{aligned}\frac{dC(t)}{dt} &= k_1 C(t) + k_3 CI(t) - k_2 C(t) \frac{I(t)}{k_8 + I(t)} - k_5 C(t) H(t) \\ \frac{dCI(t)}{dt} &= (k_1 - k_3) CI(t) + k_2 C(t) \frac{I(t)}{k_8 + I(t)} \\ \frac{dCH(t)}{dt} &= (k_1 - k_4) CH(t) + k_5 C(t) H(t) - k_2 CH(t) \frac{I(t)}{k_8 + I(t)} + k_3 CHI(t) \\ \frac{dCHI(t)}{dt} &= (k_1 - k_3 - k_4) CHI(t) + k_2 CH(t) \frac{I(t)}{k_8 + I(t)} \\ \frac{dH(t)}{dt} &= k_6 CH(t) - k_7 H(t) \\ \frac{dI(t)}{dt} &= -k_9 I(t).\end{aligned}$$

Derivation of parameter estimates.

First, the biological decay rates for HIV-1 (k_7) and IFN α (k_9) were experimentally determined separately and assumed to be invariant in the different conditions (Fig. S1). We then estimated all seven remaining parameters (k_1 through k_6 and k_8) and the initial CD4 T cell count $C_{(0)}$ using the 72h timecourse data. In particular, we estimated these parameters by minimizing the weighted sum of squared distances between each observation and the corresponding model prediction. Using our experimental data, we cannot directly distinguish between individual uninfected subspecies (C and CI) or infected subspecies (CH and CHI). Thus, the observed cell species, GFP+ and GFP- cells, were assumed to represent the sum of CH and CHI, and the sum of C and CI, respectively.

We compared the basic model (Model 1) to several variants of the model to determine which could more accurately fit the dataset, and to identify the features that make important contributions to model accuracy. For Models 1, 3 and 4, the rate of conversion

to inhibited cell states saturates due to the inclusion of the k_8 rate constant, while for models 2, 5 and 6 we take the conversion rate of C to CI and CH to CHI as linearly proportional to I, as has been done in previous models of IFN α interaction. For Model 3, cell division was restricted to uninfected CD4 T cells that had not been exposed to IFN α (C). For Model 4, we only considered the interaction of IFN α with uninfected CD4 T cells, and ignored inhibition of previously infected cells – meaning that the CHI species was eliminated from the model. For Model 5, the death rate (k_4) for the CHI species was modeled as distinct from the death rate of CH, while for Model 6, the interconversion rate constants (k_2 and k_3) between uninhibited and inhibited states were distinct for infected and uninfected cells. Different model configurations are described graphically in Figure S2.

The accuracy of the model fits were compared between these six different model configurations (Table 2). Notably, we found that inclusion of the saturation constant for IFN α -mediated inhibition dramatically improved the accuracy of the fitting, with significantly lower fit error for all model variants with saturating inhibition (Models 1, 3 and 4). Model 1 most accurately simulated overall timecourse data, and became our default model for further analysis. This model was also significantly superior to another variant with saturating inhibition that lacks CHI (Model 4) suggesting that considering the effects of IFN α on infected cells is important. Model 1 also accurately simulated important features of the timecourse data for %GFP- and GFP+ T cells, as well as the concentration of infectious HIV-1 in the supernatant (Figure 3A-C). The better fit for the saturating models was not simply due to the inclusion of an extra rate constant (k_8), because other variants of the linear inhibition model with additional parameters (models 5

and 6) did not exhibit a comparable improvement in fit quality.

Table 2: Sum of squared error for model fit versus measured species.

A nonlinear least squares method was used to fit experimental data to six different model configurations – some with saturating inhibition by IFN α (Models 1, 3 and 4), and others with linear inhibition (Models 2, 5 and 6). Weighted squared error (Fit error) was determined for the best fit for each model with respect to the all measured concentrations of GFP- cells, GFP+ cells, and HIV-1. Fit error total refers to the overall mean error of the fit to all collected data. For each model, a 95% confidence interval for the increase in error over that of Model 1 (95% CI), and the Akaike Information Criterion (AIC), are shown. An asterisk next to the fit error value for a model indicates a statistically significant difference in performance relative to Model 1, at the $p < 0.05$ level.

Model	Description	Parameters	Fit error	95% CI	AIC
1	Basic model (saturating inhibition).	8	277.5		2529
2	Linear inhibition	7	849.5*	240.7 - 984.0	3671
3	Saturating inhibition, cell division restricted to C species	8	296.6	-1.7 - 42.3	2567
4	Saturating inhibition, no effect of IFN α on infected cells (No CHI)	8	297.7*	6.6 - 35.5	2570
5	Linear inhibition, separate death rates (k_4) for CH and CHI	8	848.4*	240.1 - 985.3	3671
6	Linear inhibition, separate interconversion rates (k_2 and k_3) for uninfected (C and CI) and infected (CH and CHI) cells.	9	846.0*	240.1 - 976.3	3669

Figure 3: A saturating model of inhibition of HIV-1 by IFN α recapitulates infection timecourse data.

Experimental data for the concentration of uninfected (GFP-) cells (A), infected (GFP+) cells (B), and infectious HIV-1 (C) was fitted with a saturating model (Model 1). Open circles represent independent experimental data points, while for each species, the solid black lines represent the model's best fit. Data points with the same value are shown side by side.

Estimated parameter values for the model rate constants were determined for all six model variants (Table 3, Table S1). Estimates for most parameters except k_2 , k_3 and k_8 were similar between Model 1 (saturating) and Model 2 (linear). However, compared to Model 1, Model 2 exhibited a significantly lower k_2 estimate and a higher k_3 estimate. Also, the predicted concentrations for each individual CD4 T cell species were calculated from the best fit for both Model 1 and Model 2. Notably, for most concentrations of IFN α , Model 1 predicts a higher proportion of cells in the inhibited states compared to Model 2, although both models predict that the majority of inhibited cells are uninfected over the range of IFN α concentrations tested (Fig S4).

Table 3: Estimated model parameter values.

Values for unfixed rate constants were obtained as the best fits of Model 1 and Model 2 to the experimental dataset.

Parameter	Units	Model 1 value (95% CI)	Model 2 value (95% CI)
k1	day ⁻¹	0.905 (0.831-1.006)	0.898 (0.831-0.945)
k2	ng ⁻¹ day ⁻¹	37.5 (31.5-45.1)	0.0431 (0.0291-0.0610)
k3	day ⁻¹	261 (214-552)	355 (0-inf)
k4	day ⁻¹	6.42 (4.80-8.61)	8.13 (5.86-10.96)
k5	uL day ⁻¹ FFU ⁻¹	0.00913 (0.00736-0.0116)	0.0136 (0.0104-0.0175)
k6	FFU cell ⁻¹ day ⁻¹	20.1 (18.3-23.1)	14.4 (13.3-15.2)
k8	ng mL ⁻¹	0.154 (0.063-0.463)	NA

To further investigate the performance of our model, we re-plotted the data for HIV-1 levels, % GFP+ cells, and total cell concentration, at 3dpi, against different IFN α concentrations, and compared to model predictions (Fig. 4). Significantly, Model 1 was able to simulate key features of the HIV-1 inhibition curve accurately including plateaus at high and low IFN α levels, and a broadly sloped inhibitory curve. Furthermore, Model 1 performed better than a linear inhibition model (Model 2) in two out of the three curves, with statistically significantly lower RMSE values for HIV-1 concentrations and the percentage of infected cells.

Figure 4: Saturating effect of IFN α on CD4 T cells improves model accuracy.

Dose-response data for the effect of different IFN α concentrations on the concentration of HIV-1 (left panel), the percentage of GFP+ cells (middle panel), and on total cell concentration (right panel) from the 3dpi timepoint of the timecourse dataset were compared to model generated estimates for Models 1 and 2. Root mean squared errors (RMSE) are shown on the figure panels. Circles represent individual data points. An

asterisk besides RMSE values for Model 2 denotes a statistically significant difference in performance relative to Model 1.

Differential effects of inhibitory parameters on the potency of IFN α .

Using the saturating default model, we examined the sensitivity of biologically significant outcomes of the model to specific parameters - particularly the parameters that regulated the IFN α -related component of the network (k_2 , k_3 and k_8). To measure the outcome of parameter scanning, we calculated the HIV-1 concentration at 3dpi as a function of IFN α concentration with different parameter values over a range of 10 fold higher or lower than our estimated values. As expected, increasing the rate at which IFN α converts CD4 T cells to an inhibited state (k_2), and decreasing the reversion rate (k_3), both individually resulted in lower total HIV-1 amounts at most concentrations of IFN α (Fig 5A). Modulating the saturation rate constant (k_8) had negligible effect on HIV-1 levels at higher IFN α concentrations, but modulated the IFN α threshold at which saturation is achieved. Thus, although the inclusion of a saturation constant greatly improved accuracy of the model, the outcome of infection is less sensitive to the value of this parameter than for k_2 and k_3 at higher IFN α concentrations.

To describe the effects of IFN α on HIV-1, two metrics have previously been used – the IC₅₀, that is, the IFN α concentration that results in 50% of maximal inhibition, and the

V_{res} , which is the percent residual HIV-1 replication at the maximal IFN α concentration [31]. Based on our simulations, we observe a clear differential effect of k_2 , k_3 and k_8 on and V_{res} , namely that k_2 and k_3 strongly affect V_{res} , while k_8 does not (Fig 5B). Interestingly, increased k_2 values and decreased k_3 values both reduced the IC_{50} of IFN α , while scaling these parameters in the opposite direction had little effect. By contrast, both higher and lower k_8 values affected the IC_{50} , with lower k_8 leading to a lower IC_{50} , and higher k_8 leading to a higher IC_{50} . Overall, we conclude that V_{res} is determined by the balance of k_2 and k_3 , while IC_{50} is determined by the combined effect of k_2 , k_3 and k_8 . Thus our model makes testable predictions about how these specific network parameters affect IFN α inhibition of HIV-1.

Figure 5 Differential effects of inhibitory parameters of the potency of IFN α .

(A) Experimentally measured values for k_2 (left panel), k_3 (middle panel) and k_8 (right panel), were modulated up (blue) and down (red) by 10-fold, and the effect on the outcome of infection determined by running a simulation with these parameter values substituted for the experimentally determined ones, and calculating the concentration of infectious HIV-1 at 3dpi. (B) The effect of modulating values for k_2 , k_3 and k_8 on IC_{50} (concentration required for 50% inhibition) and V_{res} (the percent HIV-1 replication at maximal IFN α concentration) were determined by scanning parameter values over a 10 fold range above and below our measured value, and calculating the HIV-1 concentration at 3dpi.

Discussion

In this manuscript we describe, for the first time, a dynamical model that simulates the interaction of HIV-1 with IFN α , and demonstrate that this model accurately fits an experimental dataset. Also, we have estimated rate constants for how IFN α interacts with CD4 T cells and HIV-1, thereby providing a realistic range in which to perform simulations of infection. A key novel feature of this model is a saturating rate constant for IFN α 's effects on target cells, which significantly increased the accuracy of the model's fit to the experimental data. In the absence of this feature, the model performed poorly in fitting, and had a profoundly different balance of forward and reverse rate constants for the generation of inhibited cellular states (k_2 and k_3). Furthermore, we have found that a model in which IFN α affects both uninfected and infected cells fit experimental data significantly better than one in which IFN α only affected uninfected cells. Although the interaction of IFN α with viral infection has been previously studied using modeling approaches [30,32–34], a saturating rate constant for inhibition of infection has not been a standard assumption of these models. A similar study that considered inhibition of influenza by IFN α found that a linear inhibition model, in which IFN α affects uninfected cells only, was able to successfully fit experimental data, suggesting that models of IFN α interaction with viruses may require virus-specific dynamics [30].

This model could be useful for the design of novel therapies for HIV-1 that target the IFN α pathway. Notably, our model recapitulates the observation that IFN α has a broad

HIV-1-inhibition curve, meaning that changes in IFN α concentration over several orders of magnitude have only partial effects on HIV-1 levels. However, sensitivity analysis of the network rate constants indicates that modulation of the k_2 and k_3 rate constants can lead to a dramatically more potent inhibition of HIV-1 for a given IFN α concentration. By contrast, the value of the saturation rate constant (k_8) has a lesser effect on the course of infection for most IFN α concentrations. As such, our model predicts that clinical modulation of k_2 and k_3 could prove more beneficial than simply boosting total IFN α levels by a similar factor or by modulating k_8 .

In order to design therapies that can target the biological processes controlled by these rate constants, it will be critical to identify the molecules that govern them. The signaling pathway and transcriptional response to IFN α have been extensively characterized, and the identities of many of the participating molecules have been described [14]. The rate of conversion to inhibited states (k_2) could reflect features such as the abundance of the IFNAR receptor, the expression level of IFN α signaling factors such as STAT1/2 and IRF9, as well as the transcription/translation rate for antiviral effector proteins. The reversion rate (k_3), by contrast, is likely determined by the off-rate for ISGF3 detachment from the IRSE sequences in the promoters of ISGs, and/or the degradation rate for antiviral effector proteins in the cytoplasm. The requirement for a saturating rate constant (k_8) to accurately fit our dataset could reflect any rate-limiting process in the generation of an ‘inhibited’ cell. Factors that contribute to these rate constants could potentially be experimentally identified by manipulating expression of known components of this pathway, and examining the impact on the network behavior.

Novel therapies designed to target these rate constants could involve boosting or reducing the expression/activity of these key factors.

The application of this model to clinical data from HIV-1 patients could yield valuable insights into HIV-1 immunity and pathogenesis. HIV-1 infection results in a wide range of outcomes in terms of viral loads, immune responses, and disease progression. If parameter values can be derived for individual patients, these parameters could be examined for correlation with any of these clinical outcomes. For example, do non-progressors and rapid progressors have different parameter sets that can potentially contribute differences in the course of clinical infection? Some evidence suggests that this may indeed be the case - females mount an intrinsically stronger IFN α response than males, and also exhibit stronger early control of HIV-1 [35–38]. The dynamics of early acute HIV-1 infection, and the resulting innate immune response, likely contains valuable information relating to the IFN α response of individual patients that could be analyzed by a version of this model, but unfortunately, data from this phase of infection have been difficult to obtain, since most patient are not diagnosed until they have entered the chronic phase of infection.

An important consideration for IFN α -related therapy is that IFN α may play different and potentially opposing roles at different times during HIV-1 infection. Recent data suggest that while IFN α and pDCs do indeed limit HIV-1/SIV levels during early infection, they may also promote CD4 T cell depletion at later times, possibly due to IFN α -induced upregulation of apoptosis [39]. However, administration of high doses of IFN α to SIV-

infected African green monkeys, which naturally tolerate infection, does not enhance CD4 T cell loss or pathogenesis [40]. Furthermore, blockade of IFN α signaling in SIV-infected Rhesus Macaques leads to higher viral loads and more rapid disease progression [10]. Therefore, it is unclear if future models of IFN α 's role in clinical infection will have to incorporate this feature of IFN α 's behavior in order to accurately model the disease process.

Our model should also be considered in the light of some inherent caveats. For example, the model relies on mass-action interactions to simulate the innate immune response to infection. While this may accurately model responses in well-mixed compartments such as the blood, it may not be applicable to immune responses in solid tissues such as lymph nodes or mucosal surfaces. IFN α may also have additional indirect mechanisms of influencing the course of infection, such as helping to promote immune responses by Natural killer (NK) cells or lymphocytes [41,42]. Also, the results of this manuscript rely on an immortalized cell line that may behave differently than primary human CD4 T cells *in vivo*. Furthermore, HIV-1 employs several countermeasures against inhibitory ISGs, and different virus strains may exhibit differential sensitivity to IFN α [31]. Currently this model does not consider the contribution of endogenous IFN α to the course of infection. *In vivo*, the endogenous IFN α response is driven by plasmacytoid DCs (pDCs), and future development of this model to analyze clinical data from HIV-1 patients will likely require the incorporation of pDCs and endogenous IFN α . Our model also makes several assumptions that may not fully reflect details of HIV-1 infection, such as assuming that infected and uninfected CD4 T cells have equivalent division rates.

Nevertheless, this study represents the first attempt to analyze the interaction of the innate immune system with HIV-1 from a computational perspective, and demonstrates that quantitative estimates for the parameters that regulate IFN α 's potency can be derived from experimental data. As such, these findings should serve as a valuable starting point for future studies investigating the dynamics of the host innate immune response to HIV-1.

Materials and methods:

Cells and viruses.

CEM 5.25 cells and GHOST-X4 cells were obtained from Dan Littman (NYU). These cells were maintained in RPMI or DMEM media respectively with 10% fetal calf serum, glutamine, and penicillin/streptomycin. An integrated LTR-GFP cassette present in the genomic DNA of these cells facilitates expression of Green Fluorescent Protein (GFP) upon HIV-1 infection.

The HIV-1 strain used was NL4-3, a CXCR4-tropic subtype B strain [43]. The pNL4-3 plasmid was obtained from aidsreagent.org. To generate stocks of infectious virus, 10ug of plasmid was transfected into subconfluent 10cm plate of HEK-293FT cells (Invitrogen) using Mirus LT-1 reagent (Mirus Bio). At 4hrs post-transfection, medium was replaced. At 2 days post-transfection, the supernatant was harvested, clarified by low-speed centrifugation, then filtered through 0.45uM filter. The samples were then aliquoted and frozen at -80C. The titer of the stock was the determined by focus-forming assay.

For experimental infections, CEM-5.25 cultures were first exposed to IFN α for 6 hrs, then infected with NL4-3 at a multiplicity of 0.1 focus-forming unit per cell for 1hr. The virus inoculum was then removed and replaced with fresh media containing IFN α . The

infected cells were then plated in 96 well plates at approximately 100 cells/uL. At 24h intervals a small fraction of the media (10%) was removed and replaced with media containing fresh IFN α .

Focus forming assays.

GHOST-X4 cells were plated at 10000 cells per well in a 96 well plate. A ten-fold dilution series of each supernatant sample was made and 100ul of each dilution was used to inoculate GHOST-X4 cells. At 3dpi, the supernatant was removed and the cells were fixed in 4% paraformaldehyde (PFA). The plate was then analyzed by fluorescence microscopy and the number of GFP+ foci per well was counted. This was then used to calculate the concentration of focus-forming units (FFU) per mL in each of the original supernatant samples.

Flow cytometry

Cell samples from infected CEM-5.25 cultures were fixed in 2% PFA for 20 minutes, then diluted in phosphate buffered saline (PBS) and analyzed on an Accuri C6 flow cytometer. The total concentration of CD4 T cells, and the percentage of infected cells (% GFP+), was calculated for each original sample.

Interferon

Human IFN α 2a was obtained from Sigma Aldrich, reconstituted in PBS, and stored at -80C.

Computational analyses.

Model fitting, simulation, and other computational analyses were done using the Python programming language. The system of differential equations was integrated using SloppyCell [43]. Model fitting was done by solving a weighted nonlinear least squares problem. Let x_{ijlt} represent the data collected for species i at interferon level j , in replicate l at time point t . Let $y_{ijlt}(k)$ be the corresponding model prediction for that species, interferon level, and time point, with parameters k . The weighted least squares problem is to minimize the fit error:

$$C(k) = \sum_i \sum_j \sum_l \sum_t \left(\frac{y_{ijlt}(k) - x_{ijlt}}{\sigma_{ij}} \right)^2.$$

The measurement variance, σ_{ij}^2 , was estimated by first measuring the variance across replicates at each time point, and then averaging these variances over time points. The nonlinear squares problem was solved using random-restart optimization. For each random-restart run, optimization was done using the L-BFGS-B optimization routine [44,45]. Optimization was started from 25 randomly selected initial values, and then the final parameters were chosen as those that produced the lowest cost across all 25 runs.

Confidence intervals for the best-fit parameters were found using the profile likelihood method [46]. The parameter confidence intervals reported here are simultaneous 95% confidence intervals.

Model comparison was done using two complementary methods: AIC and nonparametric confidence intervals on fit error. AIC provides a model comparison that incorporates the number of parameters, but requires assuming a normal noise model. Nonparametric confidence intervals were estimated using the percentile bootstrap, so do not require any assumption about the noise distribution. To determine if a difference in fit error between two models was statistically significant at the $p < 0.05$ level, 95% confidence intervals were computed for the difference in fit errors. If this 95% confidence interval contained zero, it indicated that the difference in model fit was not statistically significant at the 0.05 level. If the confidence interval did not contain zero, it indicated that the difference in model fit was statistically significant.

References:

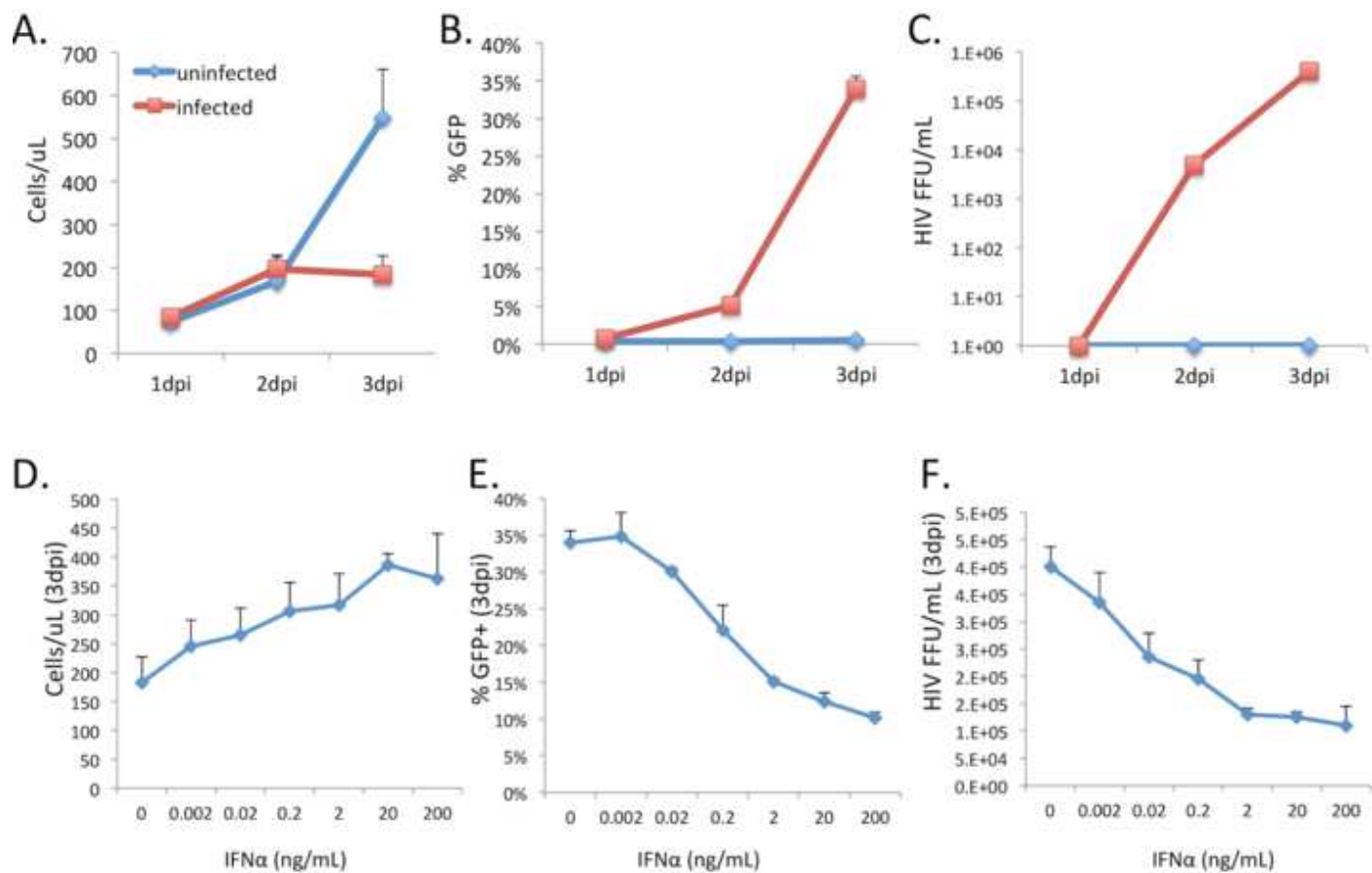
1. Bhutta ZA, Sommerfeld J, Lassi ZS, Salam RA, Das JK. Global burden, distribution, and interventions for infectious diseases of poverty. *Infect Dis Poverty*. 2014;3: 21. doi:10.1186/2049-9957-3-21
2. Archin NM, Sung JM, Garrido C, Soriano-Sarabia N, Margolis DM. Eradicating HIV-1 infection: seeking to clear a persistent pathogen. *Nat Rev Microbiol*. 2014;12: 750–764. doi:10.1038/nrmicro3352
3. Perelson AS, Ribeiro RM. Modeling the within-host dynamics of HIV infection. *BMC Biol*. 2013;11: 96. doi:10.1186/1741-7007-11-96
4. Althaus CL, Joos B, Perelson AS, Günthard HF. Quantifying the Turnover of Transcriptional Subclasses of HIV-1-Infected Cells. *PLoS Comput Biol*. 2014;10: e1003871. doi:10.1371/journal.pcbi.1003871
5. Ho DD, Neumann AU, Perelson AS, Chen W, Leonard JM, Markowitz M. Rapid turnover of plasma virions and CD4 lymphocytes in HIV-1 infection. *Nature*. 1995;373: 123–126. doi:10.1038/373123a0
6. Perelson AS, Neumann AU, Markowitz M, Leonard JM, Ho DD. HIV-1 Dynamics in Vivo: Virion Clearance Rate, Infected Cell Life-Span, and Viral Generation Time. *Science*. 1996;271: 1582–1586. doi:10.1126/science.271.5255.1582
7. Stafford MA, Corey L, Cao Y, Daar ES, Ho DD, Perelson AS. Modeling plasma virus concentration during primary HIV infection. *J Theor Biol*. 2000;203: 285–301. doi:10.1006/jtbi.2000.1076
8. Košmrlj A, Read EL, Qi Y, Allen TM, Altfeld M, Deeks SG, et al. Effects of thymic selection of the T-cell repertoire on HLA class I-associated control of HIV infection. *Nature*. 2010;465: 350–354. doi:10.1038/nature08997
9. Hardy GAD, Sieg S, Rodriguez B, Anthony D, Asaad R, Jiang W, et al. Interferon- α Is the Primary Plasma Type-I IFN in HIV-1 Infection and Correlates with Immune Activation and Disease Markers. *PLoS ONE*. 2013;8: e56527. doi:10.1371/journal.pone.0056527
10. Sandler NG, Bosinger SE, Estes JD, Zhu RTR, Tharp GK, Boritz E, et al. Type I interferon responses in rhesus macaques prevent SIV infection and slow disease progression. *Nature*. 2014;511: 601–605. doi:10.1038/nature13554
11. Iwasaki A. A Virological View of Innate Immune Recognition. *Annu Rev Microbiol*. 2012;66: 177–196. doi:10.1146/annurev-micro-092611-150203

12. Fu XY, Kessler DS, Veals SA, Levy DE, Darnell JE. ISGF3, the transcriptional activator induced by interferon alpha, consists of multiple interacting polypeptide chains. *Proc Natl Acad Sci U S A*. 1990;87: 8555–8559.
13. Levy DE, Kessler DS, Pine R, Reich N, Darnell JE. Interferon-induced nuclear factors that bind a shared promoter element correlate with positive and negative transcriptional control. *Genes Dev*. 1988;2: 383–393. doi:10.1101/gad.2.4.383
14. Schneider WM, Chevillotte MD, Rice CM. Interferon-Stimulated Genes: A Complex Web of Host Defenses. *Annu Rev Immunol*. 2014;32: 513–545. doi:10.1146/annurev-immunol-032713-120231
15. Beignon A-S, McKenna K, Skoberne M, Manches O, DaSilva I, Kavanagh DG, et al. Endocytosis of HIV-1 activates plasmacytoid dendritic cells via Toll-like receptor–viral RNA interactions. *J Clin Invest*. 2005;115: 3265–3275. doi:10.1172/JCI26032
16. Prakash A, Smith E, Lee C, Levy DE. Tissue-specific Positive Feedback Requirements for Production of Type I Interferon following Virus Infection. *J Biol Chem*. 2005;280: 18651–18657. doi:10.1074/jbc.M501289200
17. Schoggins JW, Wilson SJ, Panis M, Murphy MY, Jones CT, Bieniasz P, et al. A diverse array of gene products are effectors of the type I interferon antiviral response. *Nature*. 2011;472: 481–485. doi:10.1038/nature09907
18. Kane M, Yadav SS, Bitzegeio J, Kutluay SB, Zang T, Wilson SJ, et al. Mx2 is an interferon induced inhibitor of HIV-1 infection. *Nature*. 2013;502: 563–566. doi:10.1038/nature12653
19. Barr SD, Smiley JR, Bushman FD. The Interferon Response Inhibits HIV Particle Production by Induction of TRIM22. *PLoS Pathog*. 2008;4. doi:10.1371/journal.ppat.1000007
20. Sheehy AM, Gaddis NC, Choi JD, Malim MH. Isolation of a human gene that inhibits HIV-1 infection and is suppressed by the viral Vif protein. *Nature*. 2002;418: 646–650. doi:10.1038/nature00939
21. Neil SJD, Zang T, Bieniasz PD. Tetherin inhibits retrovirus release and is antagonized by HIV-1 Vpu. *Nature*. 2008;451: 425–430. doi:10.1038/nature06553
22. Asmuth DM, Murphy RL, Rosenkranz SL, Lertora JJJ, Kottlilil S, Cramer Y, et al. Safety, Tolerability and Mechanisms of Antiretroviral Activity of Peginterferon alfa-2a in HIV-1-Mono-infected Subjects: A Phase II Clinical Trial. *J Infect Dis*. 2010;201: 1686–1696. doi:10.1086/652420
23. Manion M, Rodriguez B, Medvik K, Hardy G, Harding CV, Schooley RT, et al. Interferon-Alpha Administration Enhances CD8+ T Cell Activation in HIV Infection. *PLoS ONE*. 2012;7. doi:10.1371/journal.pone.0030306

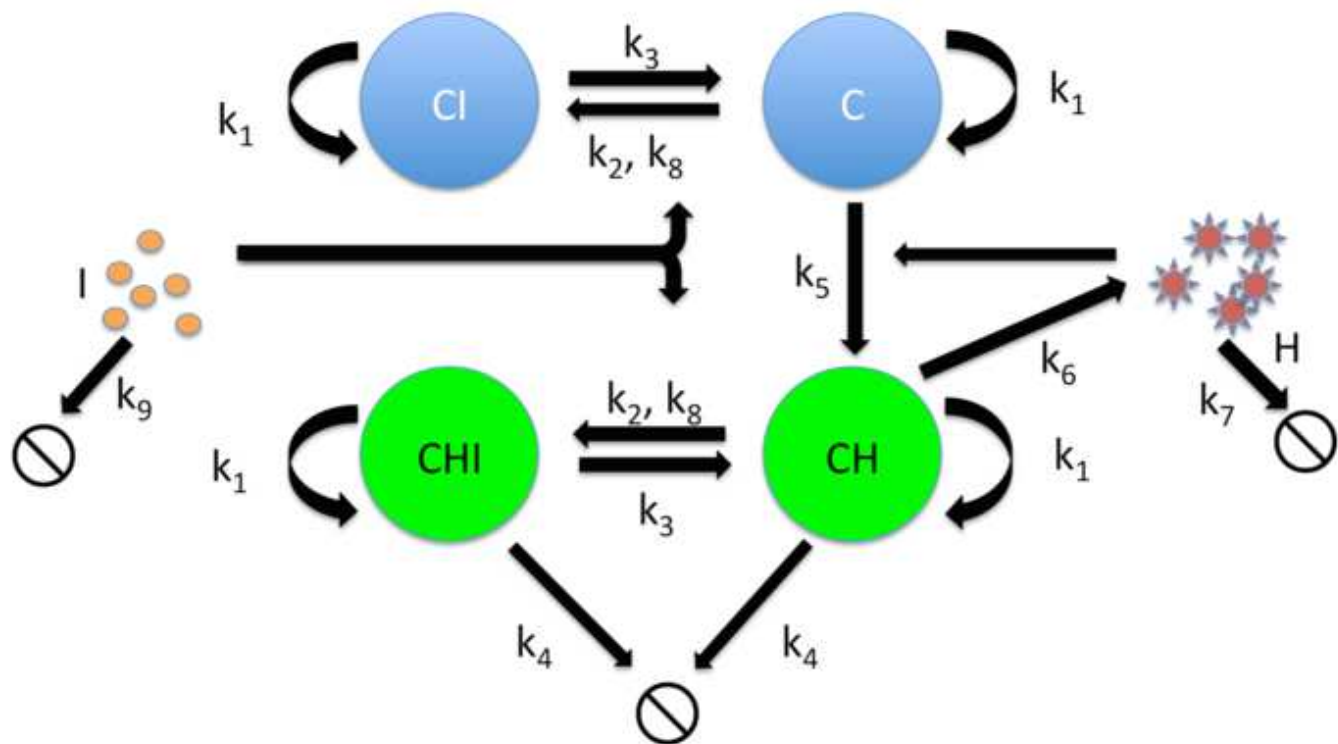
24. Azzoni L, Foulkes AS, Papasavvas E, Mexas AM, Lynn KM, Mounzer K, et al. Pegylated Interferon alfa-2a monotherapy results in suppression of HIV type 1 replication and decreased cell-associated HIV DNA integration. *J Infect Dis*. 2013;207: 213–222. doi:10.1093/infdis/jis663
25. Talal AH, Ribeiro RM, Powers KA, Grace M, Cullen C, Hussain M, et al. Pharmacodynamics of PEG-IFN alpha differentiate HIV/HCV coinfectd sustained virological responders from nonresponders. *Hepatol Baltim Md*. 2006;43: 943–953.
26. Powers KA, Dixit NM, Ribeiro RM, Golia P, Talal AH, Perelson AS. Modeling viral and drug kinetics: hepatitis C virus treatment with pegylated interferon alfa-2b. *Semin Liver Dis*. 2003;23 Suppl 1: 13–18. doi:10.1055/s-2003-41630
27. Neumann AU, Lam NP, Dahari H, Gretch DR, Wiley TE, Layden TJ, et al. Hepatitis C viral dynamics in vivo and the antiviral efficacy of interferon-alpha therapy. *Science*. 1998;282: 103–107.
28. Gervaix A, West D, Leoni LM, Richman DD, Wong-Staal F, Corbeil J. A new reporter cell line to monitor HIV infection and drug susceptibility in vitro. *Proc Natl Acad Sci*. 1997;94: 4653–4658.
29. Cecilia D, KewalRamani VN, O’Leary J, Volsky B, Nyambi P, Burda S, et al. Neutralization profiles of primary human immunodeficiency virus type 1 isolates in the context of coreceptor usage. *J Virol*. 1998;72: 6988–6996.
30. Pawelek KA, Huynh GT, Quinlivan M, Cullinane A, Rong L, Perelson AS. Modeling Within-Host Dynamics of Influenza Virus Infection Including Immune Responses. *PLoS Comput Biol*. 2012;8. doi:10.1371/journal.pcbi.1002588
31. Fenton-May AE, Dibben O, Emmerich T, Ding H, Pfafferoth K, Aasa-Chapman MM, et al. Relative resistance of HIV-1 founder viruses to control by interferon-alpha. *Retrovirology*. 2013;10: 146. doi:10.1186/1742-4690-10-146
32. Ciupe SM, Ribeiro RM, Nelson PW, Dusheiko G, Perelson AS. The role of cells refractory to productive infection in acute hepatitis B viral dynamics. *Proc Natl Acad Sci U S A*. 2007;104: 5050–5055. doi:10.1073/pnas.0603626104
33. Saenz RA, Quinlivan M, Elton D, MacRae S, Blunden AS, Mumford JA, et al. Dynamics of Influenza Virus Infection and Pathology. *J Virol*. 2010;84: 3974–3983. doi:10.1128/JVI.02078-09
34. Dahari H, Sainz B, Perelson AS, Uprichard SL. Modeling Subgenomic Hepatitis C Virus RNA Kinetics during Treatment with Alpha Interferon. *J Virol*. 2009;83: 6383–6390. doi:10.1128/JVI.02612-08
35. Addo MM, Altfeld M. Sex-based differences in HIV type 1 pathogenesis. *J Infect Dis*. 2014;209 Suppl 3: S86–92. doi:10.1093/infdis/jiu175

36. Meier A, Chang JJ, Chan ES, Pollard RB, Sidhu HK, Kulkarni S, et al. Sex differences in the TLR-mediated response of pDCs to HIV-1 are associated with higher immune activation in infected women. *Nat Med.* 2009;15: 955–959. doi:10.1038/nm.2004
37. Meier A, Chang JJ, Chan ES, Pollard RB, Sidhu HK, Kulkarni S, et al. Sex differences in the Toll-like receptor-mediated response of plasmacytoid dendritic cells to HIV-1. *Nat Med.* 2009;15: 955–959. doi:10.1038/nm.2004
38. Sterling TR, Vlahov D, Astemborski J, Hoover DR, Margolick JB, Quinn TC. Initial plasma HIV-1 RNA levels and progression to AIDS in women and men. *N Engl J Med.* 2001;344: 720–725. doi:10.1056/NEJM200103083441003
39. Fraietta JA, Mueller YM, Yang G, Boesteanu AC, Gracias DT, Do DH, et al. Type I Interferon Upregulates Bak and Contributes to T Cell Loss during Human Immunodeficiency Virus (HIV) Infection. *PLoS Pathog.* 2013;9. doi:10.1371/journal.ppat.1003658
40. Jacquelin B, Petitjean G, Kunkel D, Liovat A-S, Jochems SP, Rogers KA, et al. Innate Immune Responses and Rapid Control of Inflammation in African Green Monkeys Treated or Not with Interferon-Alpha during Primary SIVagm Infection. *PLoS Pathog.* 2014;10. doi:10.1371/journal.ppat.1004241
41. Huddleston JR, Merigan TC, Oldstone MB. Induction and kinetics of natural killer cells in humans following interferon therapy. *Nature.* 1979;282: 417–419.
42. Crouse J, Kalinke U, Oxenius A. Regulation of antiviral T cell responses by type I interferons. *Nat Rev Immunol.* 2015;15: 231–242. doi:10.1038/nri3806
43. Gutenkunst RN, Waterfall JJ, Casey FP, Brown KS, Myers CR, Sethna JP. Universally Sloppy Parameter Sensitivities in Systems Biology Models. *PLoS Comput Biol.* 2007;3: e189. doi:10.1371/journal.pcbi.0030189
44. Byrd R, Lu P, Nocedal J, Zhu C. A Limited Memory Algorithm for Bound Constrained Optimization. *SIAM J Sci Comput.* 1995;16: 1190–1208. doi:10.1137/0916069
45. Zhu C, Byrd RH, Lu P, Nocedal J. Algorithm 778: L-BFGS-B: Fortran subroutines for large-scale bound-constrained optimization. *ACM Trans Math Softw.* 1997;23: 550–560.
46. Venzon DJ, Moolgavkar SH. A Method for Computing Profile-Likelihood-Based Confidence Intervals. *J R Stat Soc Ser C Appl Stat.* 1988;37: 87–94. doi:10.2307/2347496

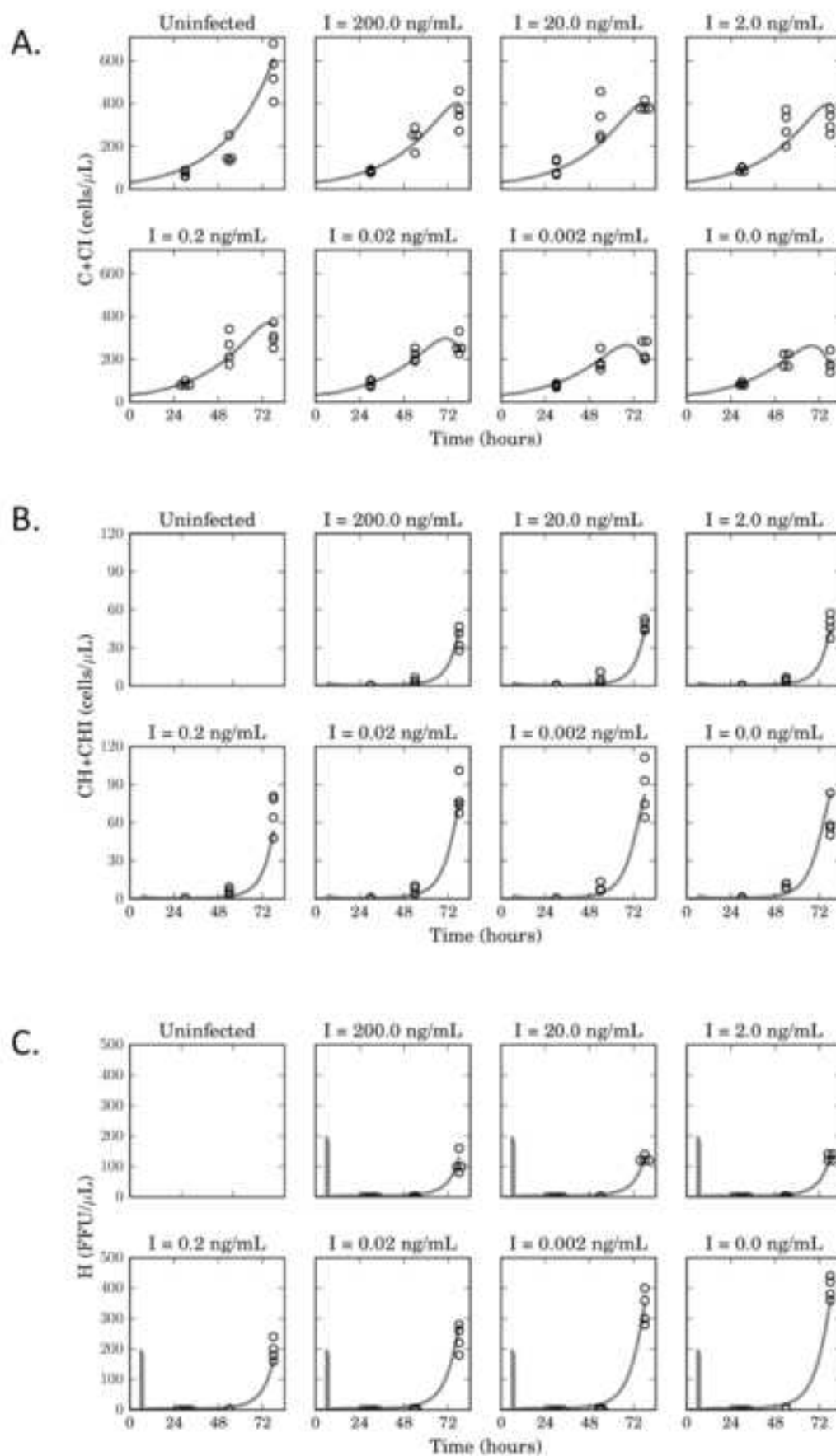
[Click here to download Figure: Fig. 1.tif](#)



[Click here to download Figure: Fig. 2.tif](#)

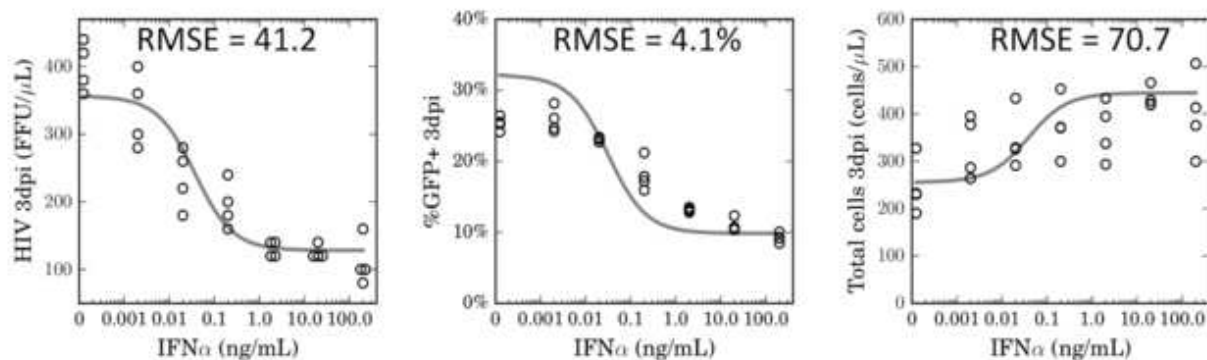


[Click here to download Figure: Fig. 3.tif](#)

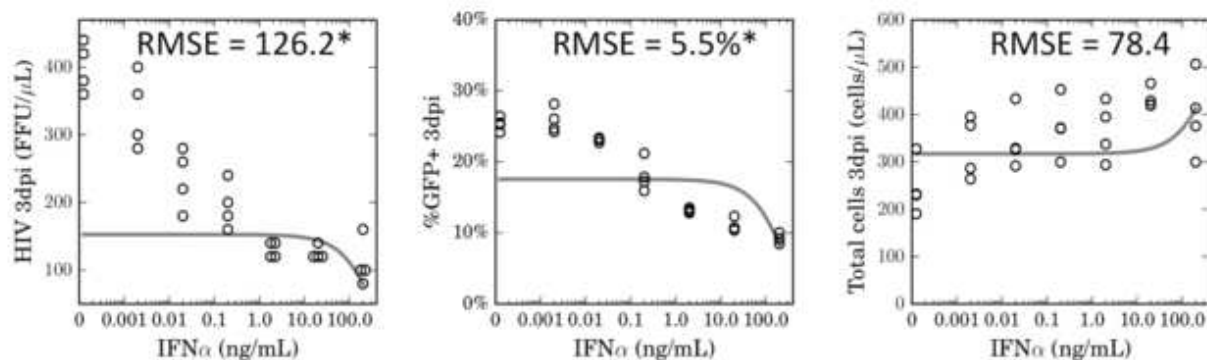


[Click here to download Figure: Fig. 4.tif](#)

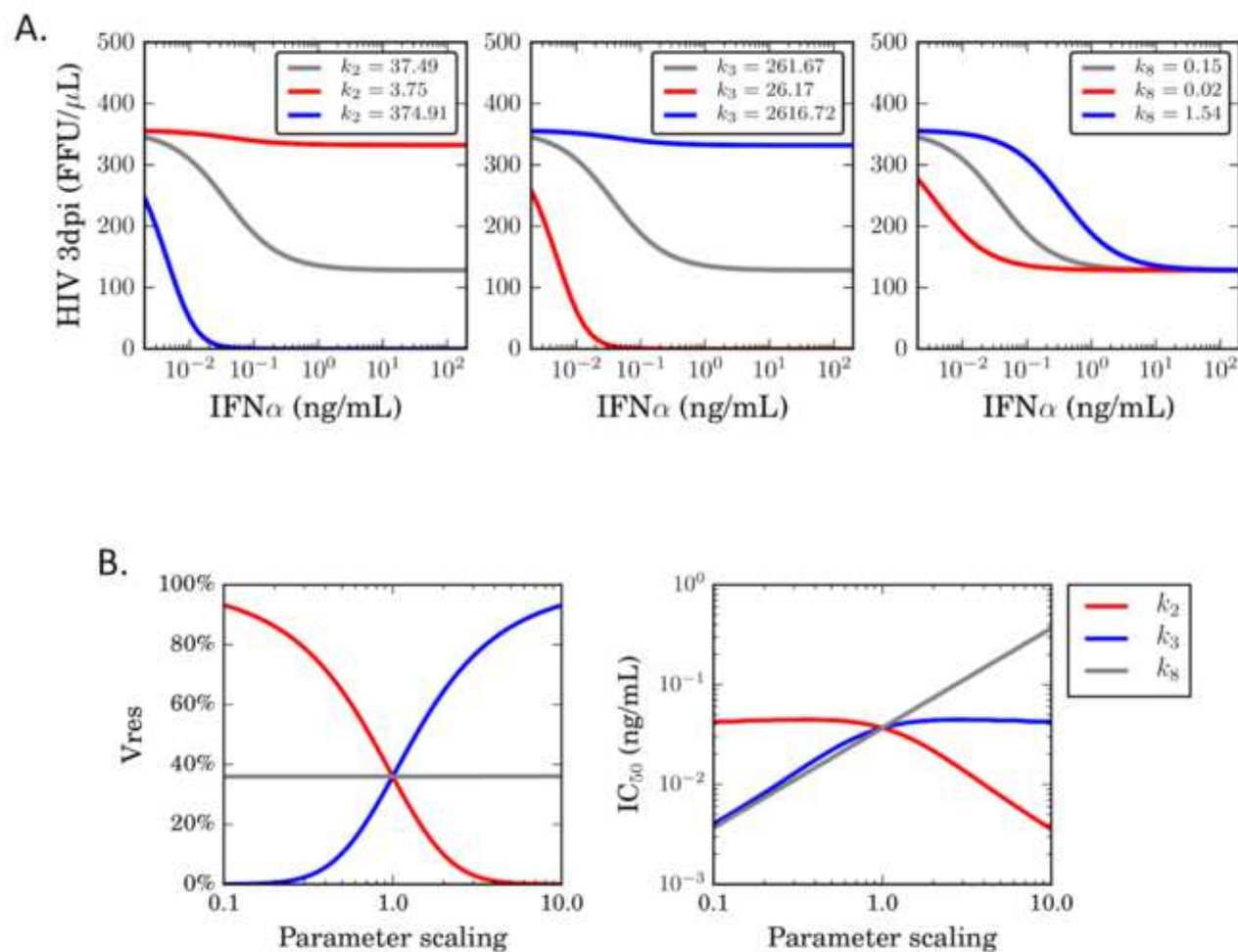
Model 1



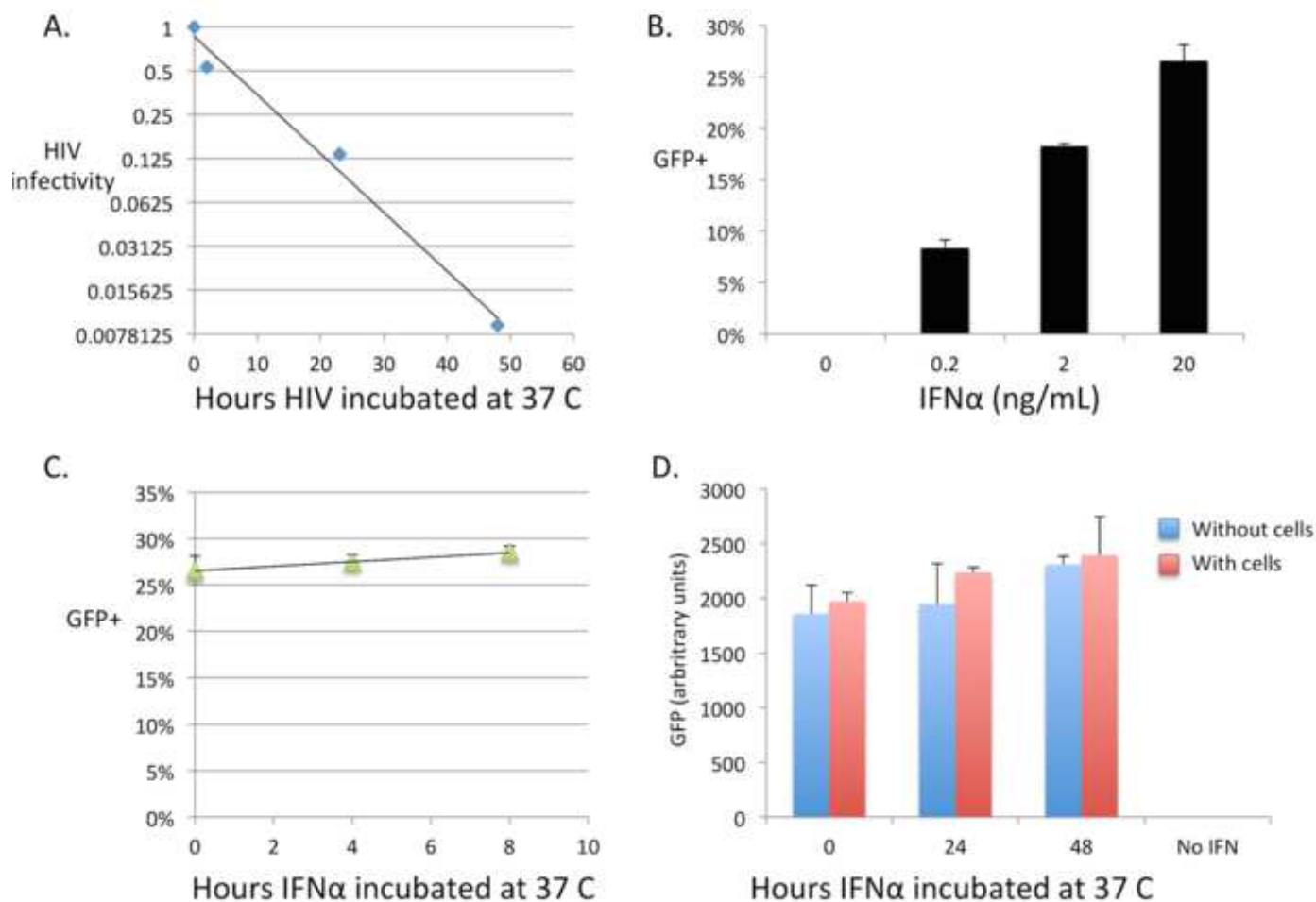
Model 2



[Click here to download Figure: Fig. 5.tif](#)

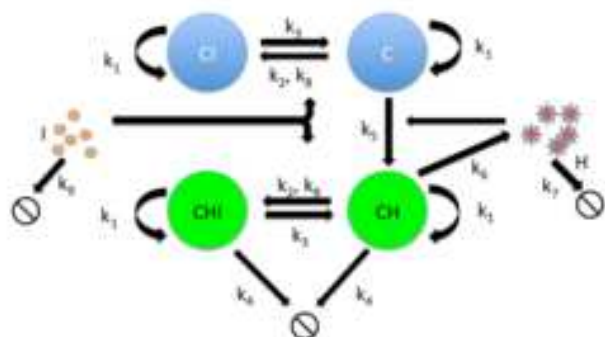


[Click here to download Figure: Fig. S1.tif](#)

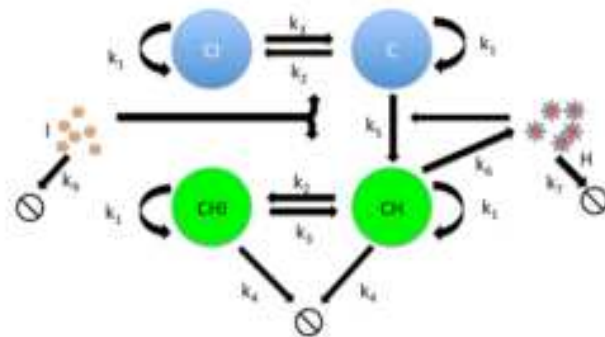


[Click here to download Figure: Fig. S2.tif](#)

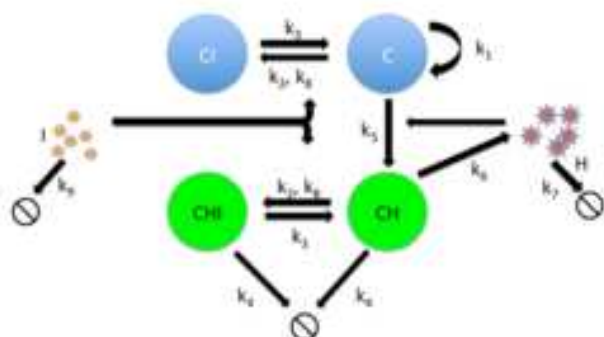
Model 1



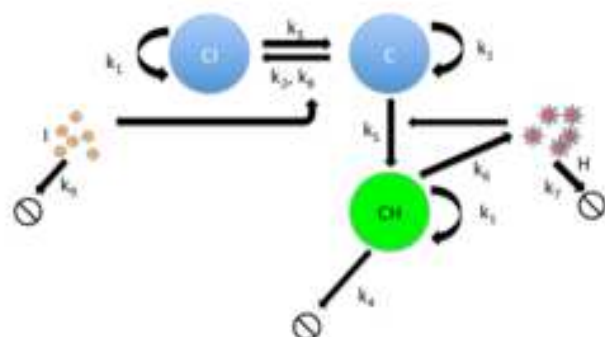
Model 2



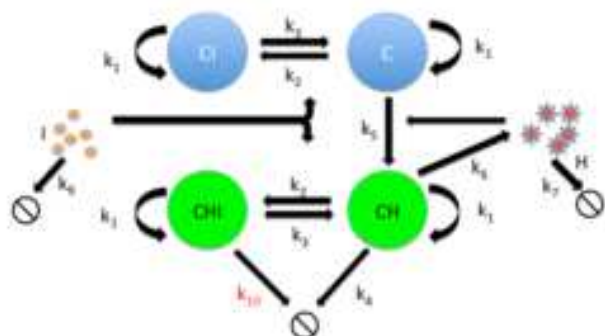
Model 3



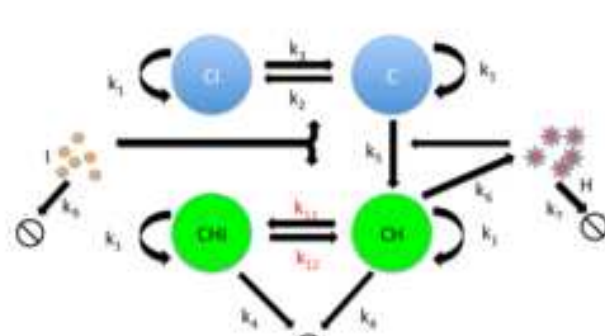
Model 4



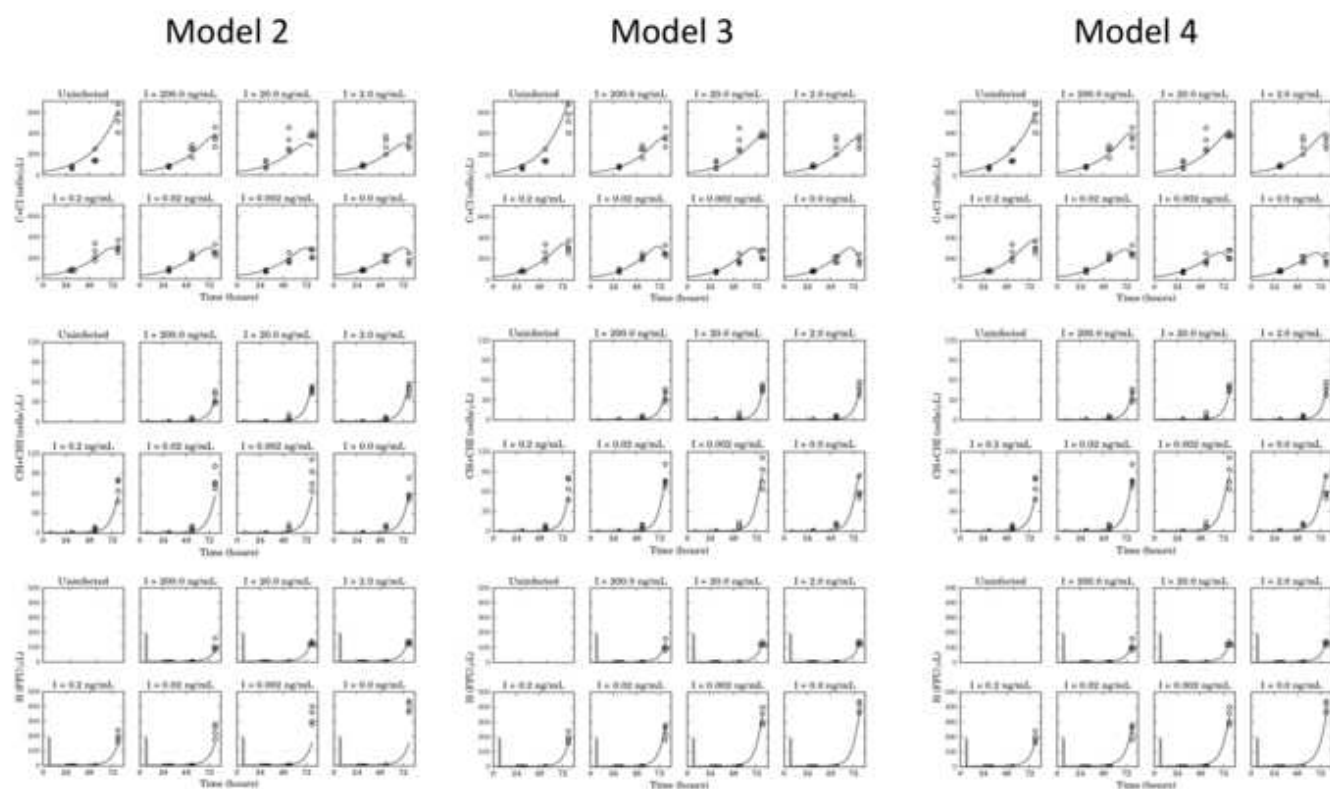
Model 5



Model 6



[Click here to download Figure: Fig. S3.tif](#)



[Click here to download Figure: Fig. S4.tif](#)

